

This paper is not submitted to IEEE Transactions on Signal Processing anymore. Since the assumptions made in this paper, e.g. "equal calibration channel magnitudes", "equal magnitudes in the transmit and receive RF gains", and "known calibration channels", were deemed too strong, we are improving the results further by relaxing all the constraints and will submit updated results later.

Thanks for reading our pre-print, all your comments are welcome.

arXiv:1709.07206v3 [eess.SP] 14 Nov 2018

Interconnection Strategies for Self-Calibration of Large Scale Antenna Arrays

Hanyu Zhu, Fuqian Yang, Zhaowei Zhu, and Xiliang Luo*

Index Terms

Calibration, self-calibration, TDD, reciprocity, Cramer-Rao Lower Bound, CRLB, massive MIMO.

Abstract

In time-division duplexing (TDD) systems, massive multiple-input multiple-output (MIMO) relies on the channel reciprocity to obtain the downlink (DL) channel state information (CSI) with the uplink (UL) CSI. In practice, the mismatches in the radio frequency (RF) analog circuits among different antennas at the base station (BS) break the end-to-end UL and DL channel reciprocity. Antenna calibration is necessary to avoid the severe performance degradation with massive MIMO. Many calibration schemes are available to compensate the RF gain mismatches and restore the channel reciprocity in TDD massive MIMO systems. In this paper, we focus on the internal self-calibration scheme where different BS antennas are interconnected via hardware transmission lines. First, we study the resulting calibration performance for an arbitrary interconnection strategy. Next, we obtain closed-form Cramer-Rao lower bound (CRLB) expressions for each interconnection strategy at the BS with only $(M - 1)$ transmission lines and M denotes the total number of BS antennas. Basing on the derived results, we further prove that the star interconnection strategy is optimal for internal self-calibration due to its lowest CRLB. In addition, we also put forward efficient recursive algorithms to derive the corresponding maximum-likelihood (ML) estimates of all the calibration coefficients. Numerical simulation results are also included to corroborate our theoretical analyses and results.

Hanyu Zhu, Fuqian Yang, Zhaowei Zhu, and Xiliang Luo (corresponding author) are with the School of Information Science and Technology, ShanghaiTech University, Shanghai 201210, China (e-mail: {zhuhy,yangfq,zhuzhw,luoxl}@shanghaitech.edu.cn).

I. INTRODUCTION

A. Massive MIMO Calibration

In massive multiple-input multiple-output (MIMO), a large number of antennas are installed at the base station (BS) to enhance the system spectral efficiencies [1]–[3]. In frequency-division duplexing (FDD) systems, mobile stations (MSs) need to feed back the downlink (DL) channel state information (CSI) to the BS in the uplink (UL) [2]. The consumed feedback overhead becomes overwhelming in massive MIMO. To avoid the need to feed back the DL CSI, time-division duplexing (TDD) is typically assumed where the channel reciprocity can be utilized to infer the DL CSI with the UL CSI at the BS [4]. However, in practice, the transmit and receive branches are composed of totally different analog circuits. Accordingly, the radio-frequency (RF) gain of the transmit chain is different from that of the receive chain at the baseband [7]. These RF gain mismatches destroy the end-to-end TDD channel reciprocity and lead to severe performance degradation in massive MIMO systems [7]–[9]. Careful calibration is thus required to compensate those RF gain mismatches at the RF front ends (FEs) to restore the channel reciprocity. Furthermore, for some applications, e.g. direction of arrival (DoA) estimation, accurate knowledge about the RF gains is also required at the BS [5], [6]. Thus antenna calibration is critical to enable efficient TDD massive MIMO.

There are two main categories of calibration schemes to compensate the RF gain mismatches. One is the “relative calibration” and the other one is the “full calibration”. The relative calibration was proposed to only restore the end-to-end UL and DL channel reciprocity without addressing the absolute phase or amplitude coherence [11]. On the other hand, the full calibration provides full absolute phase and amplitude coherence between transmitters and receivers [12].

To realize either the relative calibration or the full calibration, either the “Self-Calibration” scheme [9], [11]–[15] or the “Over-The-Air (OTA)” calibration scheme [16]–[19] can be applied. By utilizing hardware interconnections with transmission lines [10], [12]–[14] or exploiting the mutual coupling effects [9], [11], [15], the self-calibration scheme can be performed by the BS only without asking helps from the served MSs or other antenna arrays. Although the classical self-calibration scheme relying on hardware connection needs extra costly analog switches and attenuators to wire all the antenna ports together, it exhibits higher robustness and reliability in calibrating a large scale antenna array. This is due to the fact that there are no undesired effects, i.e. interference or reflections, that are picked up during the calibration phase [12]. The OTA

calibration scheme is achieved with the help of the assisting MSs or other antenna arrays [18]. In massive MIMO, the OTA calibration usually requires a significant amount of CSI feedback from the MSs [19].

B. Our Work and Contributions

The authors in [12] compared two interconnection strategies, i.e. the star interconnection and the daisy chain interconnection, for the internal self-calibration of a large scale antenna array. However, they did not provide any theoretical analyses. To the best of the authors' knowledge, there are few literatures addressing the optimal interconnection strategy to connect the antennas at the BS with transmission lines for internal self-calibration. In this paper, we investigate this interesting and fundamental problem and expect our results can serve as the design guidelines for massive MIMO systems. In particular, our main technical contributions can be summarized as follows.

- 1) We obtain the closed-form expressions for the Cramer-Rao lower bounds (CRLBs) for the calibration coefficients when an arbitrary effective interconnection strategy using $(M - 1)$ transmission lines is implemented at the BS for internal self-calibration. The derived expressions reveal how an interconnection strategy affects the calibration performance. In particular, we show the CRLB depends on the number of antennas along the shortest interconnection path between one antenna and the reference antenna;
- 2) For the first time, we prove that the star interconnection strategy is optimal in the sense that it exhibits the lowest CRLB for each calibration coefficient to be estimated. Our results can guide the designs of massive MIMO;
- 3) For both full calibration and relative calibration, with an arbitrary effective interconnection strategy implemented by the BS for internal self-calibration, we put forward efficient recursive algorithms with low complexity to derive the maximum-likelihood (ML) estimates of the unknown calibration coefficients.

C. Paper Organization and Notations

The rest of the paper is organized as follows. Section II provides some calibration preliminaries and gives the system model. Section III analyzes the CRLBs for the calibration coefficients with an arbitrary interconnection strategy. Section IV derives the closed-form CRLB expressions for one effective interconnection strategy with $(M - 1)$ interconnections and demonstrates that the

optimal interconnection strategy is the star interconnection. In Section V, we provide recursive algorithms to derive the ML estimates of the calibration coefficients. Numerical results are provided in Section VI and Section VII concludes the paper.

Notations: The imaginary unit is denoted by j . $\text{Diag}\{\cdot\}$ denotes the diagonal matrix with the diagonal elements defined inside the curly brackets. Notations $E[\cdot]$, $\text{Tr}\{\cdot\}$, $(\cdot)^T$, $(\cdot)^H$, $(\cdot)^*$, and $|\mathcal{C}|$ stand for expectation, matrix trace, transpose operation, Hermitian operation, conjugate operation, and the cardinality of the set \mathcal{C} , respectively. $\mathcal{A} \setminus \mathcal{B}$ (or $\mathcal{A} - \mathcal{B}$) means the relative complement of the set \mathcal{B} in the set \mathcal{A} . $\Re\{\cdot\}$ and $\Im\{\cdot\}$ denote the real part and imaginary part of the argument. Notations \mathbf{I}_M (\mathbf{O}_M) represents the $M \times M$ identity matrix (all zero matrix), $[\mathbf{A}]_{p,q}$ denotes the (p, q) -th entry of matrix \mathbf{A} , and $\mathbf{L}_{i,j}(l)$ denotes the elementary matrix which is the identity matrix but with an l in the (i, j) position.

II. SYSTEM MODEL AND PRELIMINARIES

A. TDD Reciprocity Calibration

A TDD massive MIMO system relies on the reciprocity between the UL and DL channels to avoid the need to ask the served MSs to feed back the DL CSIs in the UL as required by an FDD system. In particular, with the help of the UL pilots from the served MSs, the BS can acquire the UL channels and the BS can then design appropriate beamforming vectors with the UL channels due to the TDD reciprocity. In practice, the end-to-end channels also include the transceiver analog RF circuits. Due to the fact that the transmit analog branch consists of different RF circuits from the receive branch, the end-to-end channel reciprocity is broken even though the physical channel between the antennas excluding the transmit and receive circuits are still reciprocal [7]. Next we provide more preliminaries on this point.

As illustrated in Fig. 1, we consider a large scale multiuser TDD MIMO system with an M -antenna BS and K single-antenna MSs. With OFDM transmission [21], over one particular subcarrier in the DL, the received signals at the K MSs become

$$\mathbf{y}_D = \mathbf{H}_{DL} \mathbf{s}_D + \mathbf{z}_D, \quad (1)$$

where \mathbf{y}_D is a $K \times 1$ vector, $\mathbf{H}_{DL} \in \mathbb{C}^{K \times M}$ represents the end-to-end DL channel, $\mathbf{s}_D \in \mathbb{C}^{M \times 1}$ represents the precoded data vector, and \mathbf{z}_D denotes the receiver noise. Similarly, In the UL, the received signals at the BS can be expressed as

$$\mathbf{y}_U = \mathbf{H}_{UL} \mathbf{s}_U + \mathbf{z}_U, \quad (2)$$

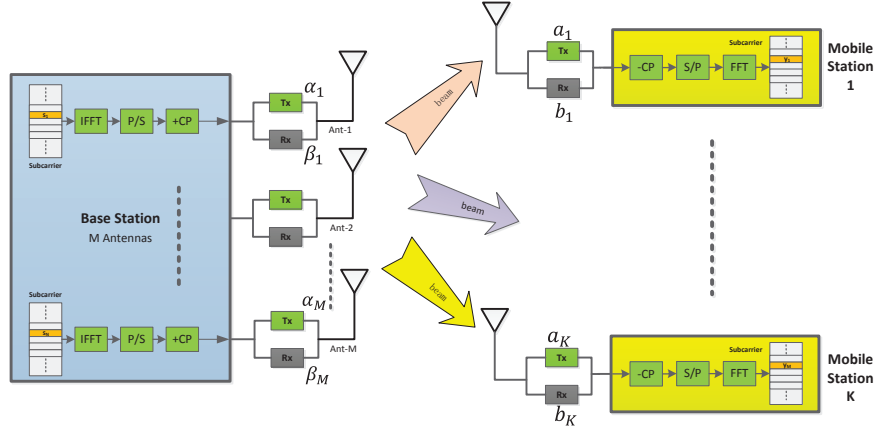


Fig. 1. Massive MIMO system illustrating different transmit and receive circuits break the TDD UL and DL channel reciprocity.

where \mathbf{y}_U is an $M \times 1$ vector, $\mathbf{H}_{UL} \in \mathbb{C}^{M \times K}$ represents the end-to-end UL channel, $\mathbf{s}_U \in \mathbb{C}^{K \times 1}$ represents the transmitted data symbols from the K MSs, and \mathbf{z}_U denotes the receiver noise at the BS. As illustrated in Fig. 1, we let $\{\alpha_m, \beta_m\}_{m=1}^M$ denote the complex-valued transmit and receive RF gains of the antennas at the BS. Meanwhile, we use $\{a_m, b_m\}_{m=1}^M$ to denote the corresponding gains of MSs' antennas. Similar to [7], [16], [18], [20], the end-to-end DL and UL channel matrices can be expressed as

$$\begin{aligned} \mathbf{H}_{DL} &= \mathbf{R}_{MS} \mathbf{H}_{PHY} \mathbf{T}_{BS}, \\ \mathbf{H}_{UL}^T &= \mathbf{T}_{MS} \mathbf{H}_{PHY} \mathbf{R}_{BS}, \end{aligned} \quad (3)$$

where $\mathbf{R}_{MS} := \text{Diag}\{b_1, b_2, \dots, b_K\}$, $\mathbf{T}_{MS} := \text{Diag}\{a_1, a_2, \dots, a_K\}$, $\mathbf{R}_{BS} := \text{Diag}\{\beta_1, \beta_2, \dots, \beta_M\}$, $\mathbf{T}_{BS} := \text{Diag}\{\alpha_1, \alpha_2, \dots, \alpha_M\}$, and \mathbf{H}_{PHY} denotes the propagating channel matrix which is reciprocal under TDD operation. From (3), we see the DL and UL channels are related as

$$\mathbf{H}_{DL} = \mathbf{R}_{MS} \mathbf{T}_{MS}^{-1} \mathbf{H}_{UL}^T \mathbf{R}_{BS}^{-1} \mathbf{T}_{BS}. \quad (4)$$

It can be observed from (4) that the UL channel and the DL channel are not reciprocal when the RF gains are different, i.e. $\mathbf{R}_{BS}^{-1} \mathbf{T}_{BS} \neq \mathbf{I}$. For DL data detection, many works have shown the RF gain mismatches at the MSs can be neglected and $\{a_m, b_m\}_{m=1}^M$ do not need to be calibrated [9], [12]. On the other hand, it is critical to carry out accurate antenna calibration at the BS. From now on, for concise notation, we write $\mathbf{R} = \mathbf{R}_{BS}$ and $\mathbf{T} = \mathbf{T}_{BS}$.

1) *Relative vs Full Calibration*: To restore the end-to-end channel reciprocity in the presence of RF gain mismatches at the BS, we need to adjust the gains of the transmit or receive chains such that we have

$$\mathbf{R}^{-1}\mathbf{C}_{\text{cal}}\mathbf{T} = s_c\mathbf{I}_M, \quad (5)$$

where $\mathbf{C}_{\text{cal}} := s_c \cdot \text{Diag}\{c_1, c_2, \dots, c_M\}$ represents the designed calibration matrix and s_c stands for the unknown scaling coefficient. From (5), we also see that we only need to know the values of relative gain coefficients, i.e. $\{c_m = \beta_m/\alpha_m\}_{m=1}^M$, to realize the end-to-end channel reciprocity. This is called “relative calibration” at the BS. For some other important applications, e.g. DoA estimation [5], [6], the BS also needs to know the absolute phase and amplitude coherence between all the transmit antennas and the receive antennas. Thus “full calibration” at the BS should be performed to obtain all the gain coefficients, i.e. $\{s_\alpha\alpha_m, s_\beta\beta_m\}_{m=1}^M$. Note we allow some unknown scaling coefficients in the estimates, i.e. s_α and s_β .

2) *OTA vs Self-Calibration*: Existing antenna calibration schemes for either full calibration or relative calibration can be put into two categories:

- Self-Calibration Method [9]–[15]: Utilizing hardware circuits connection [10], [12]–[14] or mutual coupling effects [9], [11], [15], the self-calibration method can be simply run at the BS without the need of helps from the served MSs;
- OTA Calibration Method [16]–[19]: The OTA method calibrates the BS antenna array with the OTA feedback from the served MSs or the other BSs.

Note that the OTA method works well in conventional MIMO systems. However, the amount of required CSI feedback overhead becomes overwhelming as the size of the antenna array to be calibrated becomes large [19]. On the other hand, the self-calibration method would require costly analog switches and attenuators wiring all the antenna ports together. But self-calibration scheme exhibits more robustness and reliability in calibrating a large antenna array. There are no undesired effects, i.e. interference or reflections, are picked up during the calibration phase [12].

In this paper, we focus on the full calibration approach, which delivers the estimates of all the unknown RF gain coefficients (also called calibration coefficients). Further, we will study the interconnection strategies for the internal self-calibration method which is run at the BS. We assume an internal wiring network which interconnects the transmitters and receivers of the antennas at the BS internally via transmission lines, e.g. microstrip or stripline PCB traces [12].

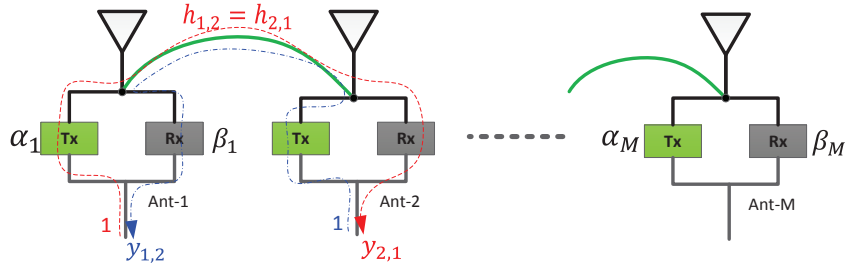


Fig. 2. Signal model for self-calibration with internal interconnection wiring. ($y_{1,2}$: the received calibration measurement at antenna-1 due to the transmission from antenna-2; $y_{2,1}$: the received calibration measurement at antenna-2 due to the transmission from antenna-1. Note the calibration channels between antenna-1 and antenna-2 are reciprocal, i.e. $h_{1,2} = h_{2,1}$.)

B. Signal Model for Internal Self-Calibration

During the calibration phase, the BS antennas transmit sounding signals over the transmission lines to obtain calibration measurements. Let $y_{p,q}$ denote the received signal at the p -th antenna due to the transmission from the q -th antenna. Without loss of generality, we assume the sounding signal is 1. We then have

$$y_{p,q} = \beta_p h_{p,q} \alpha_q + n_{p,q}, \quad (6)$$

where $h_{p,q}$ represents the gain of the calibration channel between the p -th antenna and q -th antenna and $n_{p,q}$ is additive white Gaussian noise (AWGN) with zero mean and variance σ_n^2 . See also Fig. 2. Note we have $h_{p,q} = 0$ if there is no interconnection wiring between the p -th antenna and the q -th antenna. Furthermore, we have $h_{p,q} = h_{q,p}$ due to the reciprocity of the calibration channel. By stacking all the calibration measurements in (6) together, we can have the following matrix form:

$$\mathbf{Y} = \mathbf{R}\mathbf{H}\mathbf{T} + \mathbf{N}, \quad (7)$$

where $[\mathbf{Y}]_{p,q} := y_{p,q}$, $\mathbf{R} := \text{Diag}\{\beta_1, \beta_2, \dots, \beta_M\}$, $\mathbf{T} := \text{Diag}\{\alpha_1, \alpha_2, \dots, \alpha_M\}$, $[\mathbf{H}]_{p,q} := h_{p,q}$, and $[\mathbf{N}]_{p,q} := n_{p,q}$. Note that $\mathbf{H} = \mathbf{H}^T$ since the calibration channels over each transmission line are reciprocal, i.e. $h_{p,q} = h_{q,p}$.

In this paper, we endeavor to find the optimal interconnection strategy or wiring at the BS such that different antennas are connected in the most efficient way to enable the best estimates of the calibration coefficients. To proceed with our derivations, we first make the following assumption:

- **AS-1:** All the transmission lines have the same length and damping, i.e. $h_{p,q} = h$ when the p -th antenna and the q -th antenna are interconnected.

In practice, when all the transmission lines have the same length, it could become hard to handle from the hardware implementation point of view in massive MIMO systems. For example, some particular wiring methods could lead to excessive meandering of the transmission lines to some antennas [12].

With AS-1, the calibration signal model in (7) can be simplified to

$$\mathbf{Y} = h\mathbf{R}\mathcal{A}\mathbf{T} + \mathbf{N}, \quad (8)$$

where the matrix \mathcal{A} represents the interconnection. Specifically, it is defined as

$$\mathcal{A}_{p,q} := \begin{cases} 1, & \text{Antenna-}p, q \text{ are interconnected} \\ 0, & \text{otherwise} \end{cases}. \quad (9)$$

III. PERFORMANCE ANALYSIS OF AN ARBITRARY INTERCONNECTION STRATEGY

To restore the end-to-end channel reciprocity, we only need to know the values of those transmit and receive RF gains subject to a common scaling, e.g. $\{s_\alpha\alpha_m\}_{m=1}^M$ and $\{s_\beta\beta_m\}_{m=1}^M$. In order to proceed with our quantitative analyses, we assume there is a ‘‘reference antenna’’, e.g. the f -th antenna, whose RF gains: α_f and β_f are known. The other antennas are termed ‘‘ordinary antennas’’ accordingly. For a particular interconnection strategy, given all the measurements \mathbf{Y} in (7), we can derive the corresponding CRLBs for those unknown calibration coefficients, i.e. $\{\alpha_m, \beta_m\}_{m=1}^M \setminus \{\alpha_f, \beta_f\}$. Note these CRLBs serve as the lower bounds for the variances of the estimation errors of all possible unbiased estimators [22].

Note that (7) can be rewritten in the following vector form:

$$\mathbf{y} = \boldsymbol{\mu} + \mathbf{n}, \quad (10)$$

where

$$\begin{aligned} \mathbf{y} &:= [\tilde{\mathbf{y}}_{1,2}^T, \dots, \tilde{\mathbf{y}}_{1,M}^T, \tilde{\mathbf{y}}_{2,3}^T, \dots, \tilde{\mathbf{y}}_{2,M}^T, \dots, \tilde{\mathbf{y}}_{M-1,M}^T]^T, \\ \tilde{\mathbf{y}}_{p,q} &:= [y_{p,q}, y_{q,p}]^T, \\ \boldsymbol{\mu} &:= [\tilde{\boldsymbol{\mu}}_{1,2}^T, \dots, \tilde{\boldsymbol{\mu}}_{1,M}^T, \tilde{\boldsymbol{\mu}}_{2,3}^T, \dots, \tilde{\boldsymbol{\mu}}_{2,M}^T, \dots, \tilde{\boldsymbol{\mu}}_{M-1,M}^T]^T, \\ \tilde{\boldsymbol{\mu}}_{p,q} &:= [\beta_p h_{p,q} \alpha_q, \beta_q h_{q,p} \alpha_p]^T, \end{aligned} \quad (11)$$

and \mathbf{n} is the corresponding AWGN measurement noise vector. We can define a $2(M-1)$ -by-1 vector $\tilde{\boldsymbol{\theta}}$ as

$$\tilde{\boldsymbol{\theta}} := [\boldsymbol{\alpha}^T, \boldsymbol{\beta}^T]^T, \quad (12)$$

where $\boldsymbol{\alpha} := [\alpha_1, \dots, \alpha_{f-1}, \alpha_{f+1}, \dots, \alpha_M]^T$ and $\boldsymbol{\beta} := [\beta_1, \dots, \beta_{f-1}, \beta_{f+1}, \dots, \beta_M]^T$. With the signal model in (10), the probability density function (PDF) of the measurements follows the complex Gaussian form as:

$$p(\mathbf{y}|\tilde{\boldsymbol{\theta}}) = \frac{1}{\pi^{2(M-1)} \det(\boldsymbol{\Sigma})} \exp \left\{ -(\mathbf{y} - \boldsymbol{\mu})^H \boldsymbol{\Sigma}^{-1} (\mathbf{y} - \boldsymbol{\mu}) \right\}, \quad (13)$$

where $\boldsymbol{\Sigma} = \sigma_n^2 \mathbf{I}$ is the covariance matrix of \mathbf{n} . Define the Fisher information matrix of the complex parameter $\tilde{\boldsymbol{\theta}}$ in (12) as $\mathbf{J}(\tilde{\boldsymbol{\theta}})$. Let $\bar{\mathcal{A}}$ denote the submatrix obtained by removing the f -th row and the f -th column from the interconnection matrix \mathcal{A} . Now we can establish the following result. Detailed derivations can be found in Appendix A.

Proposition 1. *Considering a BS with M antennas interconnected with a strategy \mathcal{A} , under AS-1, with the calibration signal model in (8), we can obtain the CRLB matrix for $\tilde{\boldsymbol{\theta}}$ as*

$$\text{CRLB}(\tilde{\boldsymbol{\theta}}|\mathcal{A}) = \left(\mathbf{J}(\tilde{\boldsymbol{\theta}}) \right)^{-1}, \quad (14)$$

where the Fisher information matrix $\mathbf{J}(\tilde{\boldsymbol{\theta}})$ is given by

$$\mathbf{J}(\tilde{\boldsymbol{\theta}}) = \frac{|h|^2}{\sigma_n^2} \cdot \begin{bmatrix} \mathbf{A} & \mathbf{D}^H \\ \mathbf{D} & \mathbf{B} \end{bmatrix}, \quad (15)$$

with

$$\begin{aligned} \mathbf{D} &:= \text{Diag} \{ \boldsymbol{\beta} \} \cdot \bar{\mathcal{A}} \cdot \text{Diag} \{ \boldsymbol{\alpha}^H \}, \\ \mathbf{A} &:= \text{Diag} \left\{ \sum_{i \in \mathcal{C}_1} |\beta_i|^2, \dots, \sum_{i \in \mathcal{C}_m, m \neq f} |\beta_i|^2, \dots, \sum_{i \in \mathcal{C}_M} |\beta_i|^2 \right\}, \\ \mathbf{B} &:= \text{Diag} \left\{ \sum_{i \in \mathcal{C}_1} |\alpha_i|^2, \dots, \sum_{i \in \mathcal{C}_m, m \neq f} |\alpha_i|^2, \dots, \sum_{i \in \mathcal{C}_M} |\alpha_i|^2 \right\}, \end{aligned} \quad (16)$$

and \mathcal{C}_m denotes the set of the indices of the antennas that are interconnected to the m -th antenna directly in this particular interconnection strategy \mathcal{A} .

We call the shortest interconnection path between one ordinary antenna and the reference antenna a ‘‘calibration path’’. For example, the purple path shown in Fig. 3 is the calibration path of antenna-4. To be able to estimate all the calibration coefficients, the chosen interconnection

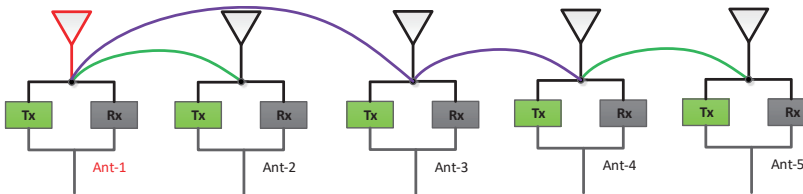


Fig. 3. The interconnection strategy with 5 antennas. Antenna-1 is chosen as the reference antenna and the purple path determine the calibration path of antenna-4.

strategy \mathcal{A} must be “effective” in the sense that there must be a calibration path between each ordinary antenna and the reference antenna. Note that in Proposition 1, to ensure that the Fisher information matrix in (15) is invertible, the interconnection strategy \mathcal{A} has to be effective.

In practice, we have a total budget of $N = N_0$ transmission lines to interconnect different antenna ports at the BS. This is due to the cost consideration and the floor plan limitation. Given N_0 transmission lines, we can find the optimal interconnection strategy \mathcal{A} by solving the following optimization problem:

$$\begin{aligned} & \underset{\mathcal{A}}{\text{minimize}} && \text{Tr} \left\{ \text{CRLB}(\tilde{\boldsymbol{\theta}}|\mathcal{A}) \right\} \\ & \text{subject to} && N = N_0. \end{aligned} \quad (17)$$

To ensure an effective interconnection strategy, we must have at least $(M - 1)$ transmission lines, i.e. we need to ensure $N_0 \geq M - 1$ in (17). In general, with N_0 transmission lines, the total number of effective interconnection strategies that can connect all the BS antennas together is finite. The optimization problem in (17) can be solved by exhaust searching. However, for a large scale antenna array, it becomes hard to handle due to the large number of antennas at the BS. In next section, we will look further into the optimization problem in (17) and obtain some insightful guidelines in designing the interconnection strategy for full calibration at the BS.

IV. OPTIMAL INTERCONNECTION STRATEGY WITH $(M - 1)$ TRANSMISSION LINES

In this section, assuming a total budget of $(M - 1)$ transmission lines to interconnect the antennas, we further examine the CRLBs for the calibration coefficients given by Proposition 1. To gain more insights from (14), we further make the following assumption:

- **AS-2:** The transmit and receive RF gains exhibit equal amplitudes, i.e. $|\alpha_m| = a$, $|\beta_m| = b$, $\forall m \in [1, M]$.

AS-2 is made here mainly due to the following concern. Constant transmit and receive amplitudes ensure identical receive signal-to-noise ratio (SNR) in the calibration measurements at each BS antenna. In general, the SNR in the received measurements will directly affect the estimation performance of the calibration coefficients. In our current study, we try to focus on the impacts of the internal interconnection strategy.

Under AS-2, we are able to obtain closed-form expressions for the CRLBs in (14). Further, we will characterize the optimal interconnection strategies for internal full calibration and relative calibration according to the derived analytical results.

A. Optimal Interconnection Strategy for Full Calibration

From now on, we assume that we have a total number of $(M - 1)$ transmission lines to deploy at the BS. From previous discussion, we know this is the least number of transmission lines that can ensure the interconnection strategy is effective. In fact, we have an M -vertex connected graph with $(M - 1)$ edges. From Theorem 2.1.4 in [23], we can readily draw the following conclusion: *the calibration path of each ordinary antenna is unique in every effective interconnection strategy with $(M - 1)$ transmission lines.*

Under AS-2, we have $|\alpha_m| = a$ and $|\beta_m| = b$. Then the Fisher information matrix in (15) can be rewritten as

$$\mathbf{J}(\tilde{\boldsymbol{\theta}}) = \frac{|h|^2}{\sigma_n^2} \cdot \begin{bmatrix} \text{Diag}\{b^2 \cdot \mathbf{t}\} & \mathbf{D}^H \\ \mathbf{D} & \text{Diag}\{a^2 \cdot \mathbf{t}\} \end{bmatrix}, \quad (18)$$

where $\mathbf{t} := [t_1, \dots, t_{f-1}, t_{f+1}, \dots, t_M]^T$ and $t_m = |\mathcal{C}_m| \geq 1$ denotes the number of antennas that are connected to the m -th antenna directly. Regarding the interconnection strategy at the BS, we can have the following useful result. The detailed proof of the following proposition is given in Appendix B.

Proposition 2. *Assuming an M -antenna BS with one reference antenna, i.e. the f -th antenna, and $(M - 1)$ ordinary antennas, for an interconnection strategy \mathcal{A} consuming $(M - 1)$ transmission lines, when some ordinary antennas are not interconnected to the reference antenna, there exists one ordinary antenna which is only connected to another ordinary antenna, i.e. $\exists n \neq f$ and $\exists u \neq f$, such that $h_{n,u} \neq 0$ and $h_{n,q} = 0, \forall q \neq u$.*

Now, let's take a look at the star interconnection strategy as shown in Fig. 4, where all the ordinary antennas are connected to the reference antenna. In this case, the Fisher information

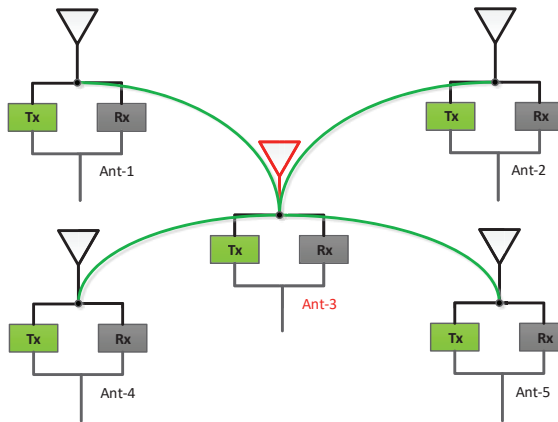


Fig. 4. The star interconnection strategy with 5 antennas. Antenna-3 is chosen as the reference antenna and all the other 4 ordinary antennas are interconnected to the reference antenna.

matrix $\mathbf{J}(\tilde{\boldsymbol{\theta}})$ becomes diagonal since $\bar{\mathbf{A}} = \mathbf{O}$. Specifically, the Fisher information matrix in (18) becomes

$$\mathbf{J}_{\text{star}}(\tilde{\boldsymbol{\theta}}) = \frac{|h|^2}{\sigma_n^2} \begin{bmatrix} \mathbf{A} & \mathbf{O} \\ \mathbf{O} & \mathbf{B} \end{bmatrix}, \quad (19)$$

where

$$\begin{aligned} \mathbf{A} &= \text{Diag} \{b^2, b^2, \dots, b^2\}, \\ \mathbf{B} &= \text{Diag} \{a^2, a^2, \dots, a^2\}. \end{aligned} \quad (20)$$

If some ordinary antennas are connected to other ordinary antennas, we see $\bar{\mathbf{A}} \neq \mathbf{O}$ and the Fisher information matrix $\mathbf{J}(\tilde{\boldsymbol{\theta}})$ is not diagonal anymore. Regarding this kind of interconnection strategies at the BS where some ordinary antennas are interconnected together, based on Proposition 2, we further establish the following useful result. See Appendix C for the proof.

Proposition 3. *Considering a BS with M antennas interconnected with a strategy $\mathcal{A}^{(k)}$ where $1 \leq W \leq M - 2$ ordinary antennas are not interconnected to the reference antenna, under AS-1 and AS-2, with the calibration signal model in (8), we can obtain an updated interconnection strategy $\mathcal{A}^{(k+1)}$ where only $(W - 1)$ ordinary antennas are not interconnected to the reference antenna directly from the strategy $\mathcal{A}^{(k)}$. In particular, in $\mathcal{A}^{(k)}$, we can find one ordinary antenna, i.e. the n_k -th antenna, which is only connected to another ordinary antenna, i.e. the u_k -th antenna. Then we just disconnect the connection to the u_k -th antenna and interconnect the n_k -th antenna to the reference antenna instead. After this update, we have the interconnection strategy*

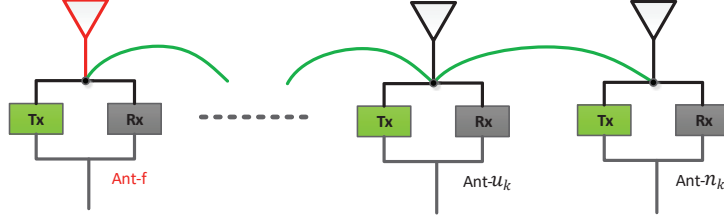


Fig. 5. The interconnection network corresponding to the interconnection strategy $\mathcal{A}^{(k)}$. The f -th antenna is chosen as the reference antenna and the n_k -th antenna is only interconnected to the u_k -th antenna.

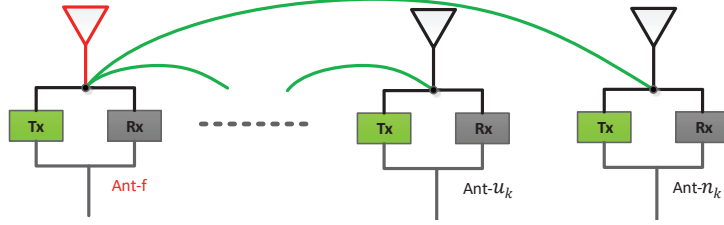


Fig. 6. The interconnection network corresponding to the interconnection strategy $\mathcal{A}^{(k+1)}$. The f -th antenna is chosen as the reference antenna and the n_k -th antenna is now interconnected to antenna- f after the update as described in Proposition 3.

$\mathcal{A}^{(k+1)}$, where $h_{n_k, u_k} = 0$ and $h_{n_k, f} \neq 0$. Furthermore, we can obtain the relationship between the Fisher information matrices for $\mathcal{A}^{(k)}$ and $\mathcal{A}^{(k+1)}$ as

$$\mathbf{J}^{(k+1)}(\tilde{\boldsymbol{\theta}}) = \mathbf{L}^{(k)} \mathbf{J}^{(k)}(\tilde{\boldsymbol{\theta}}) \mathbf{L}'^{(k)}, \quad (21)$$

where

$$\mathbf{L}^{(k)} := \mathbf{L}_{\bar{u}'_k, \bar{n}_k} \left(-\frac{\beta_u \alpha_n^*}{b^2} \right) \mathbf{L}_{\bar{u}_k, \bar{n}'_k} \left(-\frac{\beta_n^* \alpha_u}{a^2} \right), \quad (22)$$

$$\mathbf{L}'^{(k)} := \mathbf{L}_{\bar{n}'_k, \bar{u}_k} \left(-\frac{\beta_n \alpha_u^*}{a^2} \right) \mathbf{L}_{\bar{n}_k, \bar{u}'_k} \left(-\frac{\beta_u^* \alpha_n}{b^2} \right), \quad (23)$$

$\mathbf{L}_{\cdot, \cdot}(\cdot)$ represents the elementary matrix, and $\mathbf{J}^{(k)}(\tilde{\boldsymbol{\theta}})$ denotes the Fisher information matrix corresponding to the interconnection strategy $\mathcal{A}^{(k)}$. Note that \bar{n}_k and \bar{n}'_k denote the indices of the rows corresponding to α_{n_k} and β_{n_k} in $\tilde{\boldsymbol{\theta}}$ respectively and \bar{u}_k and \bar{u}'_k denote the indices of the rows corresponding to α_{u_k} and β_{u_k} in $\tilde{\boldsymbol{\theta}}$ respectively.

In Fig. 5 and Fig. 6, we have illustrated the aforementioned update in Proposition 3. By taking inverse of both sides of (21), we have the relationship between the CRLBs of the interconnection strategies $\mathcal{A}^{(k)}$ and $\mathcal{A}^{(k+1)}$, i.e.

$$\left(\mathbf{J}^{(k)}(\tilde{\boldsymbol{\theta}}) \right)^{-1} = \mathbf{L}'^{(k)} \left(\mathbf{J}^{(k+1)}(\tilde{\boldsymbol{\theta}}) \right)^{-1} \mathbf{L}^{(k)}. \quad (24)$$

Note that the CRLB matrix is updated in the reversed order in (24). Specifically, the matrix $(\mathbf{J}^{(k)}(\tilde{\boldsymbol{\theta}}))^{-1}$ is updated with the matrix $(\mathbf{J}^{(k+1)}(\tilde{\boldsymbol{\theta}}))^{-1}$.

According to Proposition 2 and Proposition 3, given the original interconnection strategy $\mathcal{A}^{(0)}$ where W ($W \in [1, M - 2]$) ordinary antennas are not interconnected to the reference antenna, we can obtain $\mathbf{J}^{(k)}(\tilde{\boldsymbol{\theta}})$ by applying k appropriate updates as shown in (21). Note that in the interconnection strategy $\mathcal{A}^{(k)}$, there are only $(W - k)$ ordinary antennas which are not interconnected to the reference antenna. Hence, after W updates, the strategy $\mathcal{A}^{(W)}$ becomes the star interconnection strategy since each antenna is interconnected to the reference antenna in $\mathcal{A}^{(W)}$. In other words, after a series of elementary transformations, we will end up with $\mathbf{J}^{(W)}(\tilde{\boldsymbol{\theta}}) = \mathbf{J}_{\text{star}}(\tilde{\boldsymbol{\theta}})$, which corresponds to the star interconnection strategy as shown in Fig. 4. Specifically, we have

$$\begin{aligned} \mathbf{J}_{\text{star}}(\tilde{\boldsymbol{\theta}}) = \mathbf{J}^{(W)}(\tilde{\boldsymbol{\theta}}) &= \mathbf{L}^{(W-1)} \dots \mathbf{L}^{(0)} \cdot \mathbf{J}^{(0)}(\tilde{\boldsymbol{\theta}}). \\ &\mathbf{L}'^{(0)} \dots \mathbf{L}'^{(W-1)}. \end{aligned} \quad (25)$$

By taking inverse of both sides of (25), we further obtain

$$\begin{aligned} \left(\mathbf{J}^{(0)}(\tilde{\boldsymbol{\theta}})\right)^{-1} &= \mathbf{L}'^{(0)} \dots \mathbf{L}'^{(W-1)} \cdot \left(\mathbf{J}_{\text{star}}(\tilde{\boldsymbol{\theta}})\right)^{-1}. \\ &\mathbf{L}^{(W-1)} \dots \mathbf{L}^{(0)}. \end{aligned} \quad (26)$$

From the result in (26), we can establish the following proposition and the proof is outlined in Appendix D.

Proposition 4. *Considering a BS with M antennas interconnected with $(M - 1)$ transmission lines, under AS-1 and AS-2, for any kind of effective interconnection strategy, the CRLBs for α_m and β_m , $\forall m \neq f$, are given by*

$$\begin{aligned} \text{CRLB}(\alpha_m) &= \frac{(d_m + 1)\sigma_n^2}{b^2 |h|^2}, \\ \text{CRLB}(\beta_m) &= \frac{(d_m + 1)\sigma_n^2}{a^2 |h|^2}, \end{aligned} \quad (27)$$

where d_m denotes the number of antennas along the calibration path between the reference antenna and the m -th antenna in addition to the reference antenna and the m -th antenna¹.

¹For the interconnection illustrated in Fig. 7, we have $d_1 = d_5 = 1$ for antenna-1 and antenna-5, $d_2 = d_4 = 0$ for antenna-2 and antenna-4.

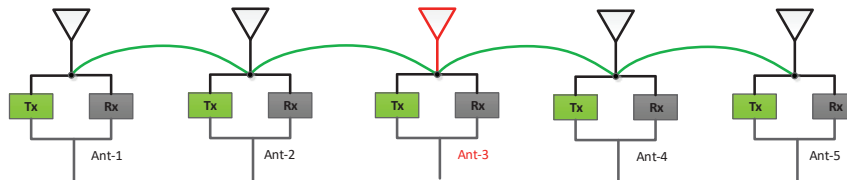


Fig. 7. The daisy chain interconnection strategy with 5 antennas with antenna-3 being selected as the reference antenna.

From Proposition 4, it can be observed that the CRLBs for the unknown parameters α_m and β_m are directly determined by the calibration path of the m -th antenna and the SNR in the corresponding calibration measurement. Furthermore, Proposition 4 provides nice closed-form results for an arbitrary interconnection strategy. For example, when the BS implements the daisy chain interconnection strategy [12] as shown in Fig. 7, where antenna- m and antenna- $(m+1)$ are interconnected, $\forall m \in [1, M-1]$, we have $d_1 = d_5 = 1$ and $d_2 = d_4 = 0$. Then the corresponding CRLBs can be computed readily according to (27).

In [12], the authors have shown the daisy chain interconnection strategy would suffer from an error propagation effect assuming noisy calibration measurements. In Proposition 4, we indeed show the error propagation effect on the calibration performance for any effective interconnection strategy with $(M-1)$ transmission lines. Specifically, the CRLBs in (27) indicate that, when the calibration path of the m -th ordinary antenna consists of more antennas, the calibration performance will decrease accordingly.

From Proposition 4, we can also easily draw the conclusion that the minimum CRLB is obtained when $d_m = 0, \forall m \neq f$. Obviously, the star interconnection strategy as shown in Fig. 4 can achieve the minimum total CRLB for the calibration coefficients, i.e.

$$\min_{\mathcal{A}} \text{Tr} \left\{ \text{CRLB}(\tilde{\theta}|\mathcal{A}) \right\} = \text{Tr} \left\{ \left(\mathbf{J}_{\text{star}}(\tilde{\theta}) \right)^{-1} \right\}. \quad (28)$$

Summarizing we can put forward the following important corollary.

Corollary 1. *Considering a BS with M antennas interconnected with $(M-1)$ transmission lines, under AS-1 and AS-2, in order to minimize the total CRLB for all the unknown calibration coefficients during internal self-calibration, we should implement the star interconnection strategy.*

Corollary 1 shows that the star interconnection strategy can achieve the minimum total CRLB for full calibration during the internal self-calibration. Thus the optimal solution of the opti-

mization problem in (17) is the star interconnection. Clearly, Corollary 1 can serve as a design philosophy for internal self-calibration in massive MIMO. In practice, compared with other interconnection strategies, the star interconnection strategy may consume more time resources for signal exchanges and longer transmission lines to interconnect the antennas.

B. Optimal Interconnection Strategy for Relative Calibration

In previous subsection, we have analyzed the optimal interconnection strategy for full calibration at the BS. In fact, similar results can be obtained in the case of relative calibration as well.

Let $c_m := \beta_m/\alpha_m$, $m \in [1, M]$, denote the relative calibration coefficients to be estimated. Assume c_f is known, i.e. the f -th antenna serves as the reference antenna. The CRLBs for the relative calibration coefficients can be obtained from the CRLBs for $\tilde{\boldsymbol{\theta}}$ [22]. In particular, we can obtain

$$\text{CRLB}(\mathbf{c}|\mathcal{A}) = \frac{\partial \mathbf{g}(\tilde{\boldsymbol{\theta}})}{\partial \tilde{\boldsymbol{\theta}}} \text{CRLB}(\tilde{\boldsymbol{\theta}}) \frac{\partial \mathbf{g}(\tilde{\boldsymbol{\theta}})^H}{\partial \tilde{\boldsymbol{\theta}}}, \quad (29)$$

where $\mathbf{c} := [c_1, \dots, c_{f-1}, c_{f+1}, \dots, c_M]^T$, the \bar{m} -th entry of $\mathbf{g}(\tilde{\boldsymbol{\theta}})$ is c_m , i.e. $g_{\bar{m}}(\tilde{\boldsymbol{\theta}}) = c_m = \beta_m/\alpha_m$, $\forall m \in \{1, \dots, f-1, f+1, \dots, M\}$, and \bar{m} denotes the index of the element c_m in \mathbf{c} . Note $\partial \mathbf{g}(\tilde{\boldsymbol{\theta}})/\partial \tilde{\boldsymbol{\theta}}$ in (29) is an $(M-1)$ -by- $2(M-1)$ Jacobian matrix whose \bar{m} -th row is $\partial g_{\bar{m}}(\tilde{\boldsymbol{\theta}})/\partial \tilde{\boldsymbol{\theta}}$. It can be verified that all the other elements are zeros except the \bar{m} -th element and the $(M + \bar{m} - 1)$ -th element in $\partial g_{\bar{m}}(\tilde{\boldsymbol{\theta}})/\partial \tilde{\boldsymbol{\theta}}$. Further, these two non-zero elements are given by

$$\begin{aligned} \frac{\partial g_{\bar{m}}(\tilde{\boldsymbol{\theta}})}{\partial \alpha_m} &= -\frac{\beta_m}{\alpha_m^2}, \\ \frac{\partial g_{\bar{m}}(\tilde{\boldsymbol{\theta}})}{\partial \beta_m} &= \frac{1}{\alpha_m}. \end{aligned} \quad (30)$$

According to the results in (27), the CRLB for the relative calibration coefficients c_m can be expressed as

$$\begin{aligned} \text{CRLB}(c_m) &= \frac{\partial g_{\bar{m}}(\tilde{\boldsymbol{\theta}})}{\partial \tilde{\boldsymbol{\theta}}} \text{CRLB}(\tilde{\boldsymbol{\theta}}) \frac{\partial g_{\bar{m}}(\tilde{\boldsymbol{\theta}})^H}{\partial \tilde{\boldsymbol{\theta}}} \\ &= \frac{b^2}{a^4} \cdot \text{CRLB}(\alpha_m) + \frac{1}{a^2} \cdot \text{CRLB}(\beta_m) \\ &= \frac{2(d_m + 1)\sigma_n^2}{a^4 |h|^2}. \end{aligned} \quad (31)$$

From the closed-form CRLB in (31), we can conclude that the star interconnection strategy is also the optimal interconnection for relative calibration.

V. EFFICIENT ESTIMATORS FOR SELF-CALIBRATION

Previously, we have derived the theoretical performance bounds for all the unbiased estimators. In this section, assuming a total budget of $(M - 1)$ transmission lines to interconnect the M antennas at the BS, under AS-1, we put forward efficient algorithms to obtain the ML estimates of the calibration coefficients for any effective interconnection strategy implemented by the BS. In order to compare with our analytical CRLBs in (27), we assume that the RF gains of the reference antenna, i.e. α_f and β_f , are given and fixed. In the meantime, the interconnection channel h is also assumed to be known. Note the interconnection channel h is time-invariant and can be estimated in advance.

A. Full Calibration

From the signal model in (8), the likelihood function of \mathbf{Y} conditioned on $\boldsymbol{\alpha}$ and $\boldsymbol{\beta}$ can be written as

$$L(\mathbf{Y}|\boldsymbol{\alpha}, \boldsymbol{\beta}) = \ln p(\mathbf{Y}|\boldsymbol{\alpha}, \boldsymbol{\beta}) = -\|\mathbf{Y} - h\mathbf{R}\mathbf{A}\mathbf{T}\|_F^2 + \xi,$$

where ξ includes those terms that do not depend on the unknown parameters. The ML estimates of the calibration coefficients $\{\alpha_m, \beta_m\}_{m=1}^M \setminus \{\alpha_f, \beta_f\}$ can be obtained by solving the following bi-convex optimization problem:

$$\begin{aligned} [\hat{\boldsymbol{\alpha}}, \hat{\boldsymbol{\beta}}] &= \arg \max_{\boldsymbol{\alpha}, \boldsymbol{\beta}} L(\mathbf{Y}|\boldsymbol{\alpha}, \boldsymbol{\beta}) \\ &= \arg \min_{\boldsymbol{\alpha}, \boldsymbol{\beta}} \|\mathbf{Y} - h\mathbf{R}\mathbf{A}\mathbf{T}\|_F^2. \end{aligned} \quad (32)$$

We can exploit the proposed recursive algorithm as Algorithm 1 to recover the variables $\boldsymbol{\alpha}$ and $\boldsymbol{\beta}$. In this algorithm, we put those s antennas whose calibration paths to the reference antenna include r antennas in addition to the reference antenna and itself into the set $\mathcal{U}_r = \{r_1, r_2, \dots, r_s\}$. Specifically, following the definition of d_m in Proposition 4, we see $d_{r_n} = r, \forall n \in [1, s]$. Also the variable p_n in Algorithm 1 denotes the index of one antenna which is in the calibration path of antenna- r_n and interconnected to the antenna- r_n directly. In Appendix E, we show that Algorithm 1 can achieve the optimal solution of the problem in (32).

For two special interconnection strategies, we can apply Algorithm 1 and obtain the following ML estimates in closed form.

- *Star Interconnection*: With calibration measurements in (6), the solution of (32) is given by

$$\hat{\alpha}_m = \frac{y_{f,m}}{h\beta_f}, \quad \hat{\beta}_m = \frac{y_{m,f}}{h\alpha_f}, \quad (33)$$

Algorithm 1 Recursive Algorithm for Full Calibration with $(M - 1)$ Transmission Lines

- 1: **Initialize** $r = 0$, $\hat{\alpha}_f = \alpha_f$, $\hat{\beta}_f = \beta_f$, and $d_{\max} = \max\{d_1, \dots, d_{f-1}, d_{f+1}, \dots, d_M\}$;
 - 2: **While** $r \leq d_{\max}$
 - 3: $s = |\mathcal{U}_r|$, $\mathcal{U}_r = \{r_1, r_2, \dots, r_s\}$, $n = 1$;
 - 4: **While** $n \leq s$
 - 5: $\hat{\alpha}_{r_n} = \frac{y_{p_n, r_n}}{h\hat{\beta}_{p_n}}$;
 - 6: $\hat{\beta}_{r_n} = \frac{y_{r_n, p_n}}{h\hat{\alpha}_{p_n}}$;
 - 7: $n = n + 1$;
 - 8: **End**
 - 9: $r = r + 1$;
 - 10: **End**
-

where $m \in \{1, 2, \dots, M\} \setminus \{f\}$. Note the corresponding mean square errors (MSEs) of the estimates in (33) are equal to the CRLB results in (27), i.e.

$$\begin{aligned} \text{MSE}(\alpha_m) &:= \text{E} [(\hat{\alpha}_m - \alpha_m)^2] = \frac{\sigma_n^2}{b^2|h|^2}, \\ \text{MSE}(\beta_m) &:= \text{E} [(\hat{\beta}_m - \beta_m)^2] = \frac{\sigma_n^2}{a^2|h|^2}; \end{aligned} \tag{34}$$

- *Daisy Chain Interconnection*: With this interconnection strategy, the ML estimates can be derived recursively as

$$\begin{aligned} \hat{\alpha}_m &= \begin{cases} \frac{y_{m+1, m}}{h\hat{\beta}_{m+1}} & m < f \\ \frac{y_{m-1, m}}{h\hat{\beta}_{m-1}} & m > f \end{cases}, \\ \hat{\beta}_m &= \begin{cases} \frac{y_{m, m+1}}{h\hat{\alpha}_{m+1}} & m < f \\ \frac{y_{m, m-1}}{h\hat{\alpha}_{m-1}} & m > f \end{cases}, \end{aligned} \tag{35}$$

where $\hat{\alpha}_f = \alpha_f$ and $\hat{\beta}_f = \beta_f$.

B. Relative Calibration

We can rewrite the signal model in (7) as

$$\begin{aligned} \mathbf{Y} &= \mathbf{C}\mathbf{T}\mathbf{H}\mathbf{T} + \mathbf{N}, \\ &= \mathbf{C}\mathbf{\Psi} + \mathbf{N}, \end{aligned} \tag{36}$$

Algorithm 2 Recursive Algorithm for Relative Calibration

- 1: **Initialize** $r = 0$, $\hat{c}_f = c_f$ and $d_{\max} = \max\{d_1, \dots, d_{f-1}, d_{f+1}, \dots, d_M\}$;
 - 2: **While** $r < d_{\max}$
 - 3: $s = |\mathcal{U}_r|$, $\mathcal{U}_r = \{r_1, r_2, \dots, r_s\}$, $n = 1$;
 - 4: **While** $n \leq s$
 - 5: $\hat{c}_{r_n} = \frac{y_{r_n, p_n}}{y_{p_n, r_n}} \hat{c}_{p_n}$;
 - 6: $n = n + 1$;
 - 7: **End**
 - 8: $r = r + 1$;
 - 9: **End**
-

where $\mathbf{C} := \text{Diag}\{c_1, c_2, \dots, c_M\}$, $c_m = \beta_m/\alpha_m$, and $\mathbf{\Psi} := \mathbf{THT}$. Similar to the full calibration in Section V-A, the ML estimates for the relative calibration coefficients $\{c_m\}_{m=1}^M \setminus \{c_f\}$ can be obtained by solving the following optimization problem [15]:

$$[\hat{\mathbf{c}}, \hat{\mathbf{\Psi}}] = \arg \min_{\mathbf{c}, \mathbf{\Psi}} \|\mathbf{Y} - \mathbf{C}\mathbf{\Psi}\|_F^2. \quad (37)$$

With the same notations as in Algorithm 1 for full calibration, we can exploit Algorithm 2 to derive the relative calibration coefficients. In Appendix F, we also show that Algorithm 2 indeed gives the optimal solution of (37). In Algorithm 2, we can see we do not require all the calibration channels to be the same for relative calibration. Moreover, we do not need to know the exact values of $h_{p,q}$. This feature has been exploited in a lot of previous research works, e.g. [9], [12], [15], [16], [18].

For two special interconnection strategies, by applying Algorithm 2, we have the following closed-form results.

- *Star Interconnection*: For star interconnection, the solution to (37) is given by

$$\hat{c}_m = \frac{y_{m,f}}{y_{f,m}} c_f, \quad (38)$$

where $m \in \{1, 2, \dots, M\} \setminus \{f\}$;

- *Daisy Chain Interconnection*: For daisy chain interconnection, the relative calibration coefficients can be estimated recursively as

$$\hat{c}_m = \begin{cases} \frac{y_{m,m+1}}{y_{m+1,m}} \hat{c}_{m+1} & m < f \\ \frac{y_{m,m-1}}{y_{m-1,m}} \hat{c}_{m-1} & m > f \end{cases}, \quad (39)$$

where $\hat{c}_f = c_f$.

C. More Comments

In [12], the authors have also exploited similar recursive algorithms to acquire the calibration coefficients. But they only considered the star interconnection and the daisy interconnection. On the other hand, our proposed recursive algorithms are more general and can efficiently solve the ML problem for an arbitrary effective interconnection strategy. Besides, we have shown that the recursive algorithms indeed generate the ML estimates.

VI. NUMERICAL RESULTS

In this section, we provide numerical results to verify our analytical results. The indices of the antennas are divided into three sets, i.e. $\mathcal{D}_1 := \{1, \dots, f - z - 1\}$, $\mathcal{D}_2 := \{f - z, \dots, f + z\}$, and $\mathcal{D}_3 := \{f + z + 1, \dots, M\}$. We define the ‘‘combined interconnection strategy’’ as the interconnection strategy where the antennas in \mathcal{D}_2 utilize the daisy chain interconnection and the antennas in \mathcal{D}_1 and \mathcal{D}_3 are interconnected to the $(f - z)$ -th and $(f + z)$ -th antennas respectively. In our simulations, we compare the star interconnection, the combined interconnection, and the daisy chain interconnection for self-calibration at the BS.

Some key parameters assumed in the simulations are listed as follows.

- The number of antennas at the BS is set to $M = 128$;
- The amplitudes of transmit and receive RF gains $\{\alpha_m, \beta_m\}_{m=1}^M$ are equal to 1, and the phases of RF gains are uniformly distributed within $[-\pi, \pi]$;
- The transmitted sounding signal is equal to 1;
- The reference antenna is the 65-th antenna, i.e. $f = 65$;
- The SNR in the calibration measurements varies from 10dB to 40dB;
- The value of z for the combined interconnection is set to 5.

In practice, we can not ensure all the transmission lines are exactly the same and all the calibration channels are identical. To take into account this factor, we assume that $h_{p,q} = h + \tilde{h}_{p,q}$ and $\tilde{h}_{p,q} \sim \mathcal{CN}(0, \sigma_h^2)$ represents the Gaussian distortions to the calibration channels. In the ideal case, we have $\sigma_h^2 = 0$.

In the case of full calibration, Fig. 8(a) shows that the star interconnection outperforms the other interconnection strategies. Meanwhile, the proposed recursive algorithm can indeed achieve the CRLB. In Fig. 8(b), we set $\sigma_h^2 = 0.001$ and the simulation results show that the imperfectness in the designs leads to performance degradation. However, we see the star interconnection is still the optimal interconnection strategy.

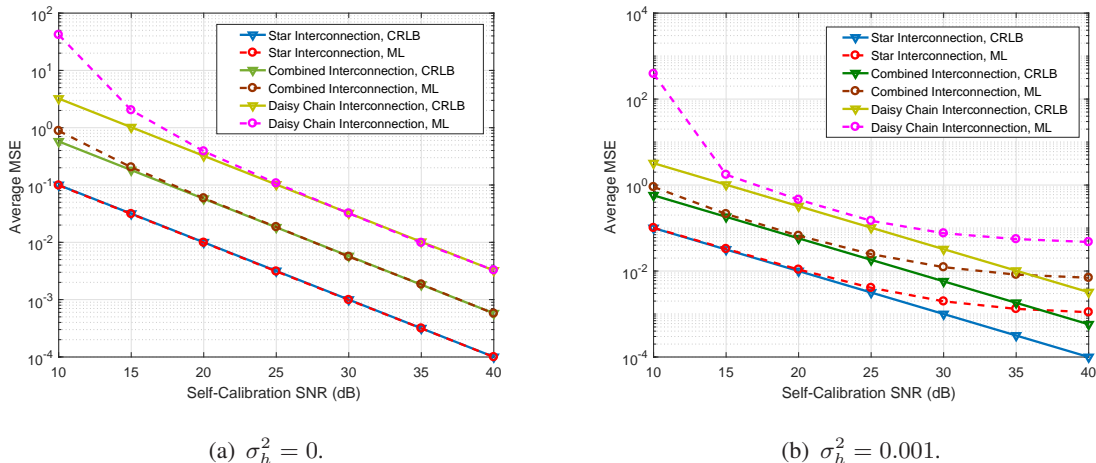


Fig. 8. Full calibration for different interconnection strategies. (“Star Interconnection”: star interconnection strategy is used for full calibration at the BS; “Combined Interconnection”: combined interconnection strategy is used for full calibration at the BS; “Daisy Chain Interconnection”: daisy chain interconnection is used for full calibration at the BS; “CRLB”: average CRLB over all the unknown calibration coefficients; “ML”: simulated average MSE of all the estimated calibration coefficients for different interconnection strategies with the proposed ML estimators in Section V.)

Fig. 9(a) and Fig. 9(b) show the relative calibration performance. The simulation results also demonstrate the star interconnection is the best interconnection strategy. Note that, in the case of relative calibration, the distortions in the calibration channels only slightly affect the estimation performance.

In order to see the effects of different interconnection strategies on the DL spectral efficiency of a massive MIMO system, we simulate a system with one BS serving $K = 6$ MSs. In (1), we set the DL receiver noise variance to 1. The DL propagation channels from the BS to the MSs are assumed to be i.i.d. complex Gaussian with unit variance, i.e. $[H_{PHY}]_{k,m} \sim \mathcal{CN}(0, 1)$. Assume that the BS carries out either match filter (MF) or zero-forcing (ZF) for DL beamforming [2]. Specifically, we can formulate the precoded data vector in (1) as $\mathbf{s}_D = \frac{1}{\sqrt{\gamma}} \mathbf{W} \mathbf{x}_D$, where \mathbf{W} contains the beamforming vectors to all K MSs, \mathbf{x}_D is a $K \times 1$ signal vector containing the transmitted symbols to each MS, and the scaling factor γ normalizes the total transmission power to 1. Assuming \mathbf{x}_D is zero mean and satisfies $\mathbb{E}[\mathbf{x}_D \mathbf{x}_D^H] = \mathbf{I}_K$, we have $\gamma = \text{Tr}\{\mathbf{W}^H \mathbf{W}\}$. Note for the MF or ZF beamforming, the corresponding precoding matrices are formed as $\mathbf{W}_{MF} = \hat{\mathbf{H}}_{DL}^H$ and $\mathbf{W}_{ZF} = \hat{\mathbf{H}}_{DL}^H (\hat{\mathbf{H}}_{DL} \hat{\mathbf{H}}_{DL}^H)^{-1}$ respectively, where $\hat{\mathbf{H}}_{DL}$ denotes the estimate of the DL channel. Assuming the BS has perfect knowledge about the UL CSIs of all the MSs, by exploiting the TDD channel reciprocity, the estimate of the DL channel is $\hat{\mathbf{H}}_{DL} =$

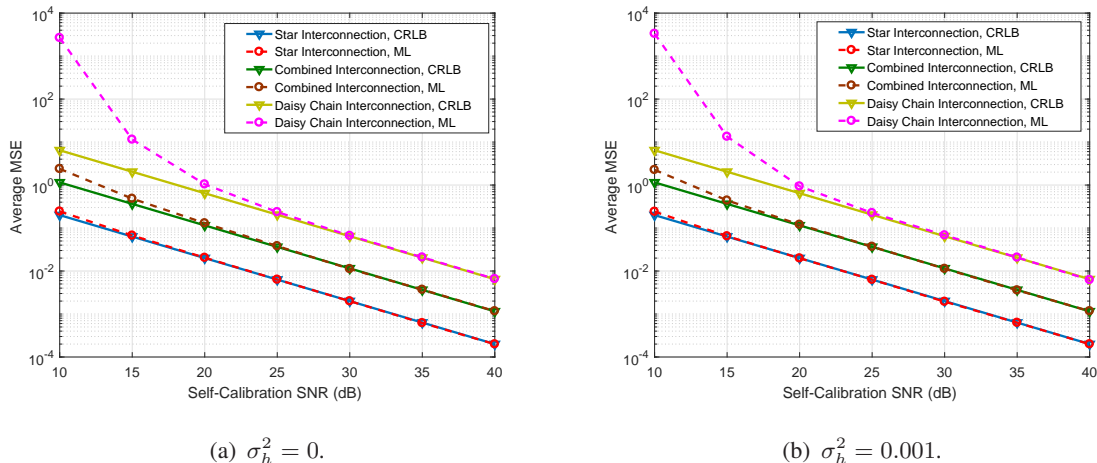


Fig. 9. Relative calibration for different interconnection strategies. (“Star Interconnection”: star interconnection strategy is used for relative calibration at the BS; “Combined Interconnection”: combined interconnection strategy is used for relative calibration at the BS; “Daisy Chain Interconnection”: daisy chain interconnection is used for relative calibration at the BS; “CRLB”: average CRLB of all the relative calibration coefficients; “ML”: simulated average MSE of all the estimated relative calibration coefficients with the ML estimators in Section V.)

\mathbf{H}_{UL}^T . In Fig. 10(a) and Fig. 10(b), we simulate the average DL spectral efficiencies when different calibration interconnection strategies are implemented at the BS. The results show that the star interconnection achieves the optimal DL spectral efficiency for both MF and ZF precoding. Meanwhile, the daisy chain interconnection strategy gives the worst DL spectral efficiency performance.

VII. CONCLUSIONS

In this paper, we have studied the interconnect strategies for internal self-calibration of the large scale antenna array at the BS. We have derived the CRLBs in estimating the unknown calibration coefficients for an arbitrary interconnect strategy. Furthermore, closed-form expressions were derived for each effective interconnection strategy with $(M - 1)$ transmission lines. Basing on the theoretical analyses, we have proved that the star interconnection is the optimal strategy to interconnect the antennas at the BS for internal self-calibration. Additionally, we have also put forward efficient recursive algorithms to compute the ML estimates of those unknown calibration coefficients. Our results in this paper offer system designers a baseline philosophy to choose appropriate interconnection strategy for self-calibration at the BS.

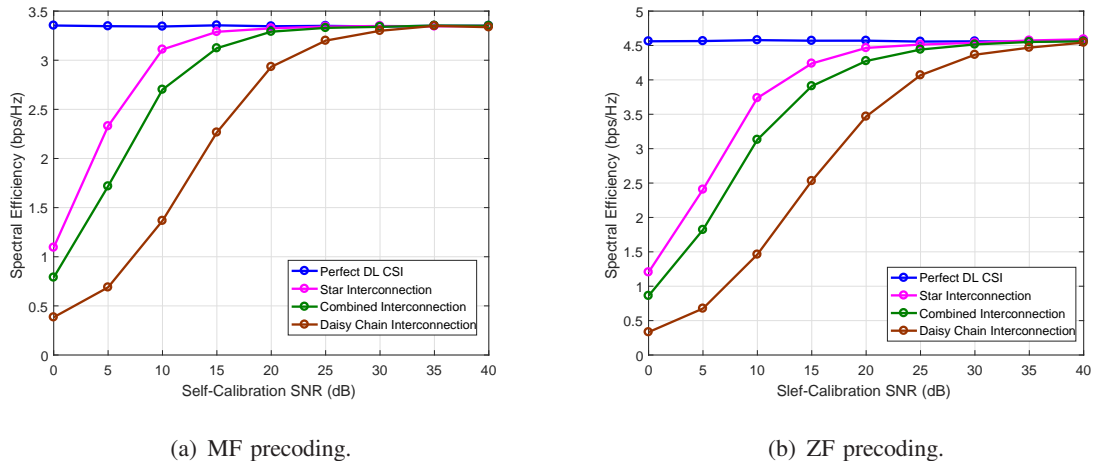


Fig. 10. Average DL spectral efficiency for different interconnection strategies with full calibration. (“Star Interconnection”: simulated average DL spectral efficiency when the star interconnection strategy is used for full calibration; “Combined Interconnection”: simulated average DL spectral efficiency when the combined interconnection strategy is used for full calibration; “Daisy Chain”: simulated average DL spectral efficiency when the daisy chain interconnection strategy is used for full calibration; “Perfect DL CSI”: simulated average DL spectral efficiency when the BS has available perfect DL CSI.)

Note in this paper, we have assumed all the transmission lines are of the same length and gain and our focus is on the optimal interconnection strategy. In our future works, we can relax these assumptions by allowing transmission lines of different lengths and seek the most economic way to interconnect all the antennas.

APPENDIX A

CRLBS FOR COMPLEX PARAMETERS

By expressing the complex numbers α_m and β_m in the form of real and imaginary parts, i.e. $\alpha_m = \alpha_m^R + j\alpha_m^I$ and $\beta_m = \beta_m^R + j\beta_m^I$, we can also define the following $4(M-1)$ -by-1 vector θ as

$$\theta := [\alpha_R^T, \beta_R^T, \alpha_I^T, \beta_I^T]^T, \quad (40)$$

where

$$\begin{aligned} \alpha_R &= [\alpha_1^R, \dots, \alpha_{f-1}^R, \alpha_{f+1}^R, \dots, \alpha_M^R]^T, \\ \beta_R &= [\beta_1^R, \dots, \beta_{f-1}^R, \beta_{f+1}^R, \dots, \beta_M^R]^T, \\ \alpha_I &= [\alpha_1^I, \dots, \alpha_{f-1}^I, \alpha_{f+1}^I, \dots, \alpha_M^I]^T, \\ \beta_I &= [\beta_1^I, \dots, \beta_{f-1}^I, \beta_{f+1}^I, \dots, \beta_M^I]^T. \end{aligned} \quad (41)$$

Define the Fisher information matrix of $\boldsymbol{\theta}$ as $\mathbf{J}(\boldsymbol{\theta})$. The (i, j) -th entry of the matrix $\mathbf{J}(\boldsymbol{\theta})$ can be obtained as [22]

$$\begin{aligned} [\mathbf{J}(\boldsymbol{\theta})]_{i,j} &= \mathbb{E} \left[\frac{\partial \ln p(\mathbf{y}|\boldsymbol{\theta})}{\partial \theta_i} \frac{\partial \ln p(\mathbf{y}|\boldsymbol{\theta})}{\partial \theta_j} \right] \\ &= \text{Tr} \left\{ \boldsymbol{\Sigma}^{-1} \frac{\partial \boldsymbol{\Sigma}}{\partial \theta_i} \boldsymbol{\Sigma}^{-1} \frac{\partial \boldsymbol{\Sigma}}{\partial \theta_j} \right\} + 2\Re \left\{ \frac{\partial \boldsymbol{\mu}^H}{\partial \theta_i} \boldsymbol{\Sigma}^{-1} \frac{\partial \boldsymbol{\mu}}{\partial \theta_j} \right\}. \end{aligned} \quad (42)$$

where $p(\mathbf{y}|\boldsymbol{\theta})$ is the complex Gaussian PDF in (13). Since $\boldsymbol{\theta}$ is not involved in $\boldsymbol{\Sigma}$, (42) can be reduced as

$$[\mathbf{J}(\boldsymbol{\theta})]_{i,j} = \frac{2}{\sigma_n^2} \Re \left\{ \frac{\partial \boldsymbol{\mu}^H}{\partial \theta_i} \frac{\partial \boldsymbol{\mu}}{\partial \theta_j} \right\}. \quad (43)$$

Meanwhile, let $\boldsymbol{\theta}_R = [\boldsymbol{\alpha}_R^T, \boldsymbol{\beta}_R^T]^T$ and $\boldsymbol{\theta}_I = [\boldsymbol{\alpha}_I^T, \boldsymbol{\beta}_I^T]^T$, then the Fisher information matrix $\mathbf{J}(\boldsymbol{\theta})$ can be rewritten as a block matrix:

$$\mathbf{J}(\boldsymbol{\theta}) = \begin{bmatrix} \mathbf{J}(\boldsymbol{\theta}_R) & \mathbf{J}(\boldsymbol{\theta}_R, \boldsymbol{\theta}_I) \\ \mathbf{J}(\boldsymbol{\theta}_I, \boldsymbol{\theta}_R) & \mathbf{J}(\boldsymbol{\theta}_I) \end{bmatrix}. \quad (44)$$

Note that

$$\begin{aligned} \mathbf{J}(\boldsymbol{\theta}_R) &= \mathbb{E} \left[\frac{\partial \ln p(\mathbf{y}|\boldsymbol{\theta})}{\partial \boldsymbol{\theta}_R} \frac{\partial \ln p(\mathbf{y}|\boldsymbol{\theta})}{\partial \boldsymbol{\theta}_R} \right] \\ &= \frac{2|h|^2}{\sigma_n^2} \cdot \begin{bmatrix} \mathbf{A} & \Re\{\mathbf{D}^H\} \\ \Re\{\mathbf{D}\} & \mathbf{B} \end{bmatrix}, \\ \mathbf{J}(\boldsymbol{\theta}_I, \boldsymbol{\theta}_R) &= \mathbb{E} \left[\frac{\partial \ln p(\mathbf{y}|\boldsymbol{\theta})}{\partial \boldsymbol{\theta}_I} \frac{\partial \ln p(\mathbf{y}|\boldsymbol{\theta})}{\partial \boldsymbol{\theta}_R} \right] \\ &= \frac{2|h|^2}{\sigma_n^2} \cdot \begin{bmatrix} \mathbf{O} & \Im\{\mathbf{D}^H\} \\ \Im\{\mathbf{D}\} & \mathbf{O} \end{bmatrix}, \end{aligned} \quad (45)$$

where

$$\begin{aligned} \mathbf{D} &= \text{Diag}\{\boldsymbol{\beta}\} \cdot \bar{\mathbf{A}} \cdot \text{Diag}\{\boldsymbol{\alpha}^H\}, \\ \mathbf{A} &= \text{Diag} \left\{ \sum_{i \in \mathcal{C}_1} |\beta_i|^2, \dots, \sum_{i \in \mathcal{C}_m, m \neq f} |\beta_i|^2, \dots, \sum_{i \in \mathcal{C}_M} |\beta_i|^2 \right\}, \\ \mathbf{B} &= \text{Diag} \left\{ \sum_{i \in \mathcal{C}_1} |\alpha_i|^2, \dots, \sum_{i \in \mathcal{C}_m, m \neq f} |\alpha_i|^2, \dots, \sum_{i \in \mathcal{C}_M} |\alpha_i|^2 \right\}, \end{aligned} \quad (46)$$

and \mathcal{C}_m denotes the set of the indices of the antennas that are interconnected to the m -th antenna directly. Accordingly, the Fisher information matrix of complex parameter $\tilde{\boldsymbol{\theta}}$ in (12) is obtained as [22]

$$\begin{aligned} \mathbf{J}(\tilde{\boldsymbol{\theta}}) &= \frac{1}{2} [\mathbf{J}(\boldsymbol{\theta}_R) + j\mathbf{J}(\boldsymbol{\theta}_I, \boldsymbol{\theta}_R)] \\ &= \frac{|h|^2}{\sigma_n^2} \cdot \begin{bmatrix} \mathbf{A} & \mathbf{D}^H \\ \mathbf{D} & \mathbf{B} \end{bmatrix}. \end{aligned} \quad (47)$$

Accordingly, we can obtain the CRLB matrix for $\tilde{\boldsymbol{\theta}}$ with the interconnection strategy \mathcal{A} as

$$\text{CRLB}(\tilde{\boldsymbol{\theta}}|\mathcal{A}) = \left(\mathbf{J}(\tilde{\boldsymbol{\theta}})\right)^{-1}. \quad (48)$$

APPENDIX B

PROOF OF PROPOSITION 2

Proof. Note that $\sum_{m=1}^M t_m = 2(M-1)$ since only $(M-1)$ transmission lines are provided. Let \mathcal{V} denote the set of the indices of the ordinary antennas that are only interconnected to the reference antenna and \mathcal{W} denote the set of the indices of the rest ordinary antennas respectively. Denote that $|\mathcal{V}| = V$ and $|\mathcal{W}| = M - V - 1$. Obviously, we have $t_v = 1, \forall v \in \mathcal{V}$ and $\sum_{v \in \mathcal{V}} t_v = V$.

Except for the star interconnection where all the ordinary antennas are interconnected to the reference antenna, we have $V < M - 1$. Note that for one particular effective interconnection strategy, at least one of the $(M - V - 1)$ ordinary antennas, e.g. the m -th antenna, $m \in \mathcal{W}$, must be interconnected to the reference antenna. Thus we must have $t_f \geq V + 1$. Furthermore, we can obtain that

$$\sum_{m \in \mathcal{W}} t_m = 2(M-1) - \sum_{v \in \mathcal{V}} t_v - t_f \leq 2M - 2V - 3. \quad (49)$$

Assuming every ordinary antenna in \mathcal{W} is interconnected to two or more other antennas, we have $t_m \geq 2, \forall m \in \mathcal{W}$. Then the following inequality must hold:

$$\sum_{m \in \mathcal{W}} t_m \geq 2|\mathcal{W}| = 2M - 2V - 2, \quad (50)$$

which is in contradiction to (49). Thus, from the definition of the set \mathcal{W} , we can conclude that there must exist one ordinary antenna in \mathcal{W} which is only interconnected to another ordinary antenna. \square

APPENDIX C

PROOF OF PROPOSITION 3

Proof. Firstly, we consider an interconnection strategy $\mathcal{A}^{(k)}$, where $1 \leq W \leq M - 2$ ordinary antennas are not interconnected to the reference antenna. According to Proposition 2, in $\mathcal{A}^{(k)}$, we can find one ordinary antenna, i.e. the n_k -th antenna, which is only connected to another ordinary antenna, i.e. the u_k -th antenna. By breaking the connection to the u_k -th antenna and interconnecting the n_k -th antenna to the reference antenna, we can obtain an updated interconnection strategy $\mathcal{A}^{(k+1)}$. Clearly, only $(W - 1)$ ordinary antennas are not interconnected to the reference antenna directly in the strategy $\mathcal{A}^{(k+1)}$.

There are two facts about the interconnection strategies $\mathcal{A}^{(k)}$ and $\mathcal{A}^{(k+1)}$ worth noting. The first fact is that the Fisher information matrix $\mathbf{J}^{(k)}(\tilde{\boldsymbol{\theta}})$ only differs from the matrix $\mathbf{J}^{(k+1)}(\tilde{\boldsymbol{\theta}})$ in six elements. Specifically, these six elements include two diagonal elements in the positions (\bar{u}_k, \bar{u}_k) and (\bar{u}'_k, \bar{u}'_k) , and four non-diagonal elements in the positions (\bar{n}_k, \bar{u}'_k) , (\bar{u}_k, \bar{n}'_k) , (\bar{u}'_k, \bar{n}_k) , and (\bar{n}'_k, \bar{u}_k) . The second fact is that the four non-diagonal elements of $\mathbf{J}^{(k+1)}(\tilde{\boldsymbol{\theta}})$ in the rows: \bar{n}_k , \bar{n}'_k and columns: \bar{n}_k , \bar{n}'_k are zeros.

Thanks to the special structure of $\mathbf{J}^{(k)}(\tilde{\boldsymbol{\theta}})$, only two diagonal elements in the positions (\bar{u}_k, \bar{u}_k) and (\bar{u}'_k, \bar{u}'_k) are changed when we apply elementary transformations to the matrix $\mathbf{J}^{(k)}(\tilde{\boldsymbol{\theta}})$ to null the aforementioned four non-diagonal elements. Specifically, we can carry out the matrix elementary transformations as $\mathbf{L}^{(k)} \mathbf{J}^{(k)}(\tilde{\boldsymbol{\theta}}) \mathbf{L}'^{(k)}$, where

$$\mathbf{L}^{(k)} := \mathbf{L}_{\bar{u}'_k, \bar{n}_k} \left(-\frac{\beta_u \alpha_n^*}{b^2} \right) \mathbf{L}_{\bar{u}_k, \bar{n}'_k} \left(-\frac{\beta_n^* \alpha_u}{a^2} \right), \quad (51)$$

$$\mathbf{L}'^{(k)} := \mathbf{L}_{\bar{n}'_k, \bar{u}_k} \left(-\frac{\beta_n \alpha_u^*}{a^2} \right) \mathbf{L}_{\bar{n}_k, \bar{u}'_k} \left(-\frac{\beta_u^* \alpha_n}{b^2} \right). \quad (52)$$

It can be verified that the matrix $\mathbf{J}^{(k)}(\tilde{\boldsymbol{\theta}})$ becomes equal to $\mathbf{J}^{(k+1)}(\tilde{\boldsymbol{\theta}})$ after the above elementary transformations, i.e. $\mathbf{J}^{(k+1)}(\tilde{\boldsymbol{\theta}}) = \mathbf{L}^{(k)} \mathbf{J}^{(k)}(\tilde{\boldsymbol{\theta}}) \mathbf{L}'^{(k)}$. \square

APPENDIX D

PROOF OF PROPOSITION 4

Proof. Let d_m represent the number of intermediate antennas along the calibration path between the reference antenna and the m -th antenna in the original interconnection strategy $\mathcal{A}^{(0)}$. Starting from $\mathcal{A}^{(k)}$, $k \in [0, W - 1]$, we will have one new interconnection strategy $\mathcal{A}^{(k+1)}$ by performing the k -th update in (21) as described in Proposition 3. Clearly, we have $(W - k)$ ordinary antennas

in $\mathcal{A}^{(k)}$ which are not interconnected to the reference antenna. Let antenna- n_k be the identified ordinary antenna that is only interconnected to the antenna- u_k in the interconnection strategy $\mathcal{A}^{(k)}$. First, we can obtain the following two intermediate results:

- 1) The relationship between the CRLBs corresponding to the interconnection strategies $\mathcal{A}^{(k)}$ and $\mathcal{A}^{(k+1)}$ is described by (24). Due to the special structure of the elementary matrices, the diagonal elements of $(\mathbf{J}^{(k)}(\tilde{\boldsymbol{\theta}}))^{-1}$ are the same as those of $(\mathbf{J}^{(k+1)}(\tilde{\boldsymbol{\theta}}))^{-1}$ except the \bar{n}_k -th and the \bar{n}'_k -th diagonal elements which are given by

$$\begin{aligned} \left[(\mathbf{J}^{(k)}(\tilde{\boldsymbol{\theta}}))^{-1} \right]_{\bar{n}_k, \bar{n}_k} &= \left[(\mathbf{J}^{(k+1)}(\tilde{\boldsymbol{\theta}}))^{-1} \right]_{\bar{n}_k, \bar{n}_k} \\ &+ \frac{a^2}{b^2} \cdot \left[(\mathbf{J}^{(k+1)}(\tilde{\boldsymbol{\theta}}))^{-1} \right]_{\bar{u}'_k, \bar{u}'_k}, \\ \left[(\mathbf{J}^{(k)}(\tilde{\boldsymbol{\theta}}))^{-1} \right]_{\bar{n}'_k, \bar{n}'_k} &= \left[(\mathbf{J}^{(k+1)}(\tilde{\boldsymbol{\theta}}))^{-1} \right]_{\bar{n}'_k, \bar{n}'_k} \\ &+ \frac{b^2}{a^2} \cdot \left[(\mathbf{J}^{(k+1)}(\tilde{\boldsymbol{\theta}}))^{-1} \right]_{\bar{u}_k, \bar{u}_k}. \end{aligned} \quad (53)$$

The notations \bar{n}_k , \bar{n}'_k , \bar{u}_k and \bar{u}'_k are defined as in (22).

- 2) From the results in (53), we can see the \bar{n}_k -th and \bar{n}'_k -th diagonal elements get updated only when we derive the CRLB matrix $(\mathbf{J}^{(k)}(\tilde{\boldsymbol{\theta}}))^{-1}$ from $(\mathbf{J}^{(k+1)}(\tilde{\boldsymbol{\theta}}))^{-1}$. This is due to the fact that $n_{k'} \neq n_k, \forall k' \neq k$. Hence, $\forall r \in (0, W - k)$, we see the \bar{n}_k -th and \bar{n}'_k -th diagonal elements of the CRLB matrix $(\mathbf{J}^{(k+r)}(\tilde{\boldsymbol{\theta}}))^{-1}$ are the same as those in the CRLB matrix $(\mathbf{J}^{(W)}(\tilde{\boldsymbol{\theta}}))^{-1} = (\mathbf{J}_{\text{star}}(\tilde{\boldsymbol{\theta}}))^{-1}$. It then follows that, $\forall r \in (0, W - k)$,

$$\begin{aligned} \left[(\mathbf{J}^{(k+r)}(\tilde{\boldsymbol{\theta}}))^{-1} \right]_{\bar{n}_k, \bar{n}_k} &= \frac{\sigma_n^2}{b^2|h|^2}, \\ \left[(\mathbf{J}^{(k+r)}(\tilde{\boldsymbol{\theta}}))^{-1} \right]_{\bar{n}'_k, \bar{n}'_k} &= \frac{\sigma_n^2}{a^2|h|^2}. \end{aligned} \quad (54)$$

In the mean time, when $0 < r \leq k$, we also see the \bar{n}_k -th and \bar{n}'_k -th diagonal elements of the CRLB matrix $(\mathbf{J}^{(k-r)}(\tilde{\boldsymbol{\theta}}))^{-1}$ are the same as those in $(\mathbf{J}^{(k)}(\tilde{\boldsymbol{\theta}}))^{-1}$. So we can get, $\forall r \in (0, k]$,

$$\begin{aligned} \left[(\mathbf{J}^{(k-r)}(\tilde{\boldsymbol{\theta}}))^{-1} \right]_{\bar{n}_k, \bar{n}_k} &= \left[(\mathbf{J}^{(k)}(\tilde{\boldsymbol{\theta}}))^{-1} \right]_{\bar{n}_k, \bar{n}_k}, \\ \left[(\mathbf{J}^{(k-r)}(\tilde{\boldsymbol{\theta}}))^{-1} \right]_{\bar{n}'_k, \bar{n}'_k} &= \left[(\mathbf{J}^{(k)}(\tilde{\boldsymbol{\theta}}))^{-1} \right]_{\bar{n}'_k, \bar{n}'_k}. \end{aligned} \quad (55)$$

With the above two intermediate results, we can apply the method of mathematical induction to complete the proof as follows.

• When $d_m = 0$, we see $m \notin \{n_0, n_1, \dots, n_{W-1}\}$ and the \bar{m} -th and \bar{m}' -th diagonal elements of the CRLB matrix $\left(\mathbf{J}^{(0)}(\tilde{\boldsymbol{\theta}})\right)^{-1}$ are not changed when we obtain it from the CRLB matrix $\left(\mathbf{J}_{\text{star}}(\tilde{\boldsymbol{\theta}})\right)^{-1}$. Note that \bar{m} and \bar{m}' denote the indices of the rows corresponding to α_m and β_m in $\tilde{\boldsymbol{\theta}}$ respectively. Thus the CRLBs for the parameters α_m and β_m are given by

$$\begin{aligned} \text{CRLB}(\alpha_m) &= \left[\left(\mathbf{J}_{\text{star}}(\tilde{\boldsymbol{\theta}})\right)^{-1} \right]_{\bar{m}, \bar{m}} = \frac{\sigma_n^2}{b^2|h|^2}, \\ \text{CRLB}(\beta_m) &= \left[\left(\mathbf{J}_{\text{star}}(\tilde{\boldsymbol{\theta}})\right)^{-1} \right]_{\bar{m}', \bar{m}'} = \frac{\sigma_n^2}{a^2|h|^2}. \end{aligned} \quad (56)$$

• When $d_m = 1$, we have $m = n_k$ and $d_{u_k} = 0$ for one particular k in $[0, W - 1]$. By applying the results in (55), we can further obtain

$$\left[\left(\mathbf{J}^{(0)}(\tilde{\boldsymbol{\theta}})\right)^{-1} \right]_{\bar{n}_k, \bar{n}_k} = \left[\left(\mathbf{J}^{(k)}(\tilde{\boldsymbol{\theta}})\right)^{-1} \right]_{\bar{n}_k, \bar{n}_k}. \quad (57)$$

With (53), the above result can be rewritten as

$$\begin{aligned} \left[\left(\mathbf{J}^{(0)}(\tilde{\boldsymbol{\theta}})\right)^{-1} \right]_{\bar{n}_k, \bar{n}_k} &= \left[\left(\mathbf{J}^{(k+1)}(\tilde{\boldsymbol{\theta}})\right)^{-1} \right]_{\bar{n}_k, \bar{n}_k} \\ &+ \frac{a^2}{b^2} \cdot \left[\left(\mathbf{J}^{(k+1)}(\tilde{\boldsymbol{\theta}})\right)^{-1} \right]_{\bar{u}'_k, \bar{u}'_k}, \end{aligned} \quad (58)$$

where $\left[\left(\mathbf{J}^{(k+1)}(\tilde{\boldsymbol{\theta}})\right)^{-1} \right]_{\bar{n}_k, \bar{n}_k} = \frac{\sigma_n^2}{b^2|h|^2}$ due to (54) and $\left[\left(\mathbf{J}^{(k+1)}(\tilde{\boldsymbol{\theta}})\right)^{-1} \right]_{\bar{u}'_k, \bar{u}'_k} = \frac{\sigma_n^2}{a^2|h|^2}$ due to the fact that $d_{u_k} = 0$ and the result in (56). Then (58) can be rewritten as

$$\text{CRLB}(\alpha_m) = \left[\left(\mathbf{J}^{(0)}(\tilde{\boldsymbol{\theta}})\right)^{-1} \right]_{\bar{n}_k, \bar{n}_k} = \frac{2\sigma_n^2}{b^2|h|^2}.$$

Similarly, we can obtain the result for β_m as

$$\text{CRLB}(\beta_m) = \left[\left(\mathbf{J}^{(0)}(\tilde{\boldsymbol{\theta}})\right)^{-1} \right]_{\bar{n}'_k, \bar{n}'_k} = \frac{2\sigma_n^2}{b^2|h|^2}.$$

• We assume Proposition 4 is true for each ordinary antenna with $s \geq 1$ additional antennas along its calibration path. For antenna- m with $d_m = s + 1$, we can have one particular k in $[0, W - 1]$ and $r \geq 1$ such that $n_k = m$, $u_k = n_{k+r}$, and $d_{u_k} = d_{n_{k+r}} = d_m - 1 = s$. By applying the results in (53)-(55), we can obtain

$$\begin{aligned} \text{CRLB}(\alpha_m) &= \left[\left(\mathbf{J}^{(0)}(\tilde{\boldsymbol{\theta}})\right)^{-1} \right]_{\bar{n}_k, \bar{n}_k} \\ &= \left[\left(\mathbf{J}^{(k+1)}(\tilde{\boldsymbol{\theta}})\right)^{-1} \right]_{\bar{n}_k, \bar{n}_k} + \frac{a^2}{b^2} \cdot \left[\left(\mathbf{J}^{(k+1)}(\tilde{\boldsymbol{\theta}})\right)^{-1} \right]_{\bar{u}'_k, \bar{u}'_k} \\ &= \frac{(d_m + 1)\sigma_n^2}{b^2|h|^2}, \end{aligned}$$

where we have utilized the fact that $[(\mathbf{J}^{(k+1)}(\tilde{\boldsymbol{\theta}}))^{-1}]_{\bar{n}_k, \bar{n}_k} = \frac{\sigma_n^2}{b^2|h|^2}$ due to (54) and our starting assumption. Specifically, due to the result in (55), we have

$$\begin{aligned} \left[(\mathbf{J}^{(k+1)}(\tilde{\boldsymbol{\theta}}))^{-1} \right]_{\bar{u}'_k, \bar{u}'_k} &= \left[(\mathbf{J}^{(k+1)}(\tilde{\boldsymbol{\theta}}))^{-1} \right]_{\bar{n}'_{k+r}, \bar{n}'_{k+r}} \\ &= \left[(\mathbf{J}^{(k+r)}(\tilde{\boldsymbol{\theta}}))^{-1} \right]_{\bar{n}'_{k+r}, \bar{n}'_{k+r}}. \end{aligned}$$

Since $d_{n_{k+r}} = s$, according to our starting assumption, we have $[(\mathbf{J}^{(k+r)}(\tilde{\boldsymbol{\theta}}))^{-1}]_{\bar{n}'_{k+r}, \bar{n}'_{k+r}} = \frac{(s+1)\sigma_n^2}{a^2|h|^2}$. Similarly, we can obtain the CRLB for β_m as

$$\text{CRLB}(\beta_m) = \frac{(d_m + 1)\sigma_n^2}{a^2|h|^2}.$$

Thus Proposition 4 is also true for each ordinary antenna with $(s + 1)$ additional antennas along its calibration path. \square

APPENDIX E

ML ESTIMATOR FOR FULL CALIBRATION

Let $d_{\max} = \max\{d_1, \dots, d_{f-1}, d_{f+1}, \dots, d_M\}$. The optimization problem in (32) can be rewritten as

$$\begin{aligned} [\hat{\boldsymbol{\alpha}}, \hat{\boldsymbol{\beta}}] &= \arg \min_{\boldsymbol{\alpha}, \boldsymbol{\beta}} \sum_{r=0}^{d_{\max}} \sum_{n=1}^{|\mathcal{U}_r|} (|y_{r_n, p_n} - \beta_{r_n} h \alpha_{p_n}|^2 \\ &\quad + |y_{p_n, r_n} - \beta_{p_n} h \alpha_{r_n}|^2), \end{aligned} \quad (59)$$

where $r_n \in \mathcal{U}_r$.

When $r = 0$, we have $p_n = f$ for $n = 1, 2, \dots, |\mathcal{U}_r|$. According to Algorithm 1, we can estimate α_{r_n} and β_{r_n} as

$$\hat{\alpha}_{r_n} = \frac{y_{f, r_n}}{h \hat{\beta}_f}, \quad \hat{\beta}_{r_n} = \frac{y_{r_n, f}}{h \hat{\alpha}_f}. \quad (60)$$

Thus, for $r = 0$, from (59) and (60), we have

$$\sum_{n=1}^{|\mathcal{U}_r|} (|y_{r_n, f} - \hat{\beta}_{r_n} h \hat{\alpha}_f|^2 + |y_{f, r_n} - \beta_f h \hat{\alpha}_{r_n}|^2) = 0. \quad (61)$$

Similarly, when $r \geq 1$, according to Algorithm 1, we can estimate α_{r_n} and β_{r_n} as

$$\hat{\alpha}_{r_n} = \frac{y_{p_n, r_n}}{h \hat{\beta}_{p_n}}, \quad \hat{\beta}_{r_n} = \frac{y_{r_n, p_n}}{h \hat{\alpha}_{p_n}}. \quad (62)$$

Accordingly, we have the following equality:

$$\sum_{n=1}^{|\mathcal{U}_r|} \left(|y_{r_n, p_n} - \hat{\beta}_{r_n} h \hat{\alpha}_{p_n}|^2 + |y_{p_n, r_n} - \hat{\beta}_{p_n} h \hat{\alpha}_{r_n}|^2 \right) = 0. \quad (63)$$

From (61), (63), we have $\|\mathbf{Y} - \mathbf{RHT}\|_F^2 = 0$ and the object function in (32) achieves the minimum since $\|\mathbf{Y} - \mathbf{RHT}\|_F^2 \geq 0$.

APPENDIX F

ML ESTIMATOR FOR RELATIVE CALIBRATION

Let $d_{\max} = \max\{d_1, \dots, d_{f-1}, d_{f+1}, \dots, d_M\}$. The optimization problem in (37) can be rewritten as

$$[\hat{\alpha}, \hat{\beta}] = \arg \min_{\alpha, \beta} \sum_{r=0}^{d_{\max}} \sum_{n=1}^{|\mathcal{U}_r|} \left(|y_{p_n, r_n} - c_{p_n} h \Psi_{p_n, r_n}|^2 + |y_{r_n, p_n} - c_{r_n} h \Psi_{r_n, p_n}|^2 \right), \quad (64)$$

where $r_n \in \mathcal{U}_r$ and $\Psi_{r_n, p_n} = \Psi_{p_n, r_n}$.

In Algorithm 2, if $r = 0$, we have $p_n = f$ for $n = 1, 2, \dots, |\mathcal{U}_r|$, and we estimate c_{r_n} and $\Psi_{r_n, f}$ as

$$\hat{\Psi}_{r_n, f} = \frac{y_{f, r_n}}{c_f h}, \quad \hat{c}_{r_n} = \frac{y_{r_n, f}}{h \hat{\Psi}_{r_n, f}} = \frac{y_{r_n, f}}{y_{f, r_n}} c_f. \quad (65)$$

Thus, for $r = 0$, from (64) and (65), we have

$$\sum_{n=1}^{|\mathcal{U}_r|} \left(|y_{f, r_n} - c_f h \hat{\Psi}_{f, r_n}|^2 + |y_{r_n, f} - \hat{c}_{r_n} h \Psi_{r_n, f}|^2 \right) = 0. \quad (66)$$

When $r \geq 1$, according to the algorithm 2, we can estimate c_{r_n} and Ψ_{r_n, p_n} as

$$\hat{\Psi}_{r_n, p_n} = \frac{y_{p_n, r_n}}{\hat{c}_{p_n} h}, \quad \hat{c}_{r_n} = \frac{y_{r_n, p_n}}{h \hat{\Psi}_{r_n, p_n}} = \frac{y_{r_n, p_n}}{y_{p_n, r_n}} \hat{c}_{r_n}. \quad (67)$$

Then we can have the following equality:

$$\sum_{n=1}^{|\mathcal{U}_r|} \left(|y_{p_n, r_n} - \hat{c}_{p_n} h \hat{\Psi}_{p_n, r_n}|^2 + |y_{r_n, p_n} - \hat{c}_{r_n} h \hat{\Psi}_{r_n, p_n}|^2 \right) = 0. \quad (68)$$

From (66) and (68), we have $\|\mathbf{Y} - \mathbf{C\Psi}\|_F^2 = 0$ and the object function in (32) achieves the minimum since $\|\mathbf{Y} - \mathbf{C\Psi}\|_F^2 \geq 0$.

REFERENCES

- [1] E. G. Larsson, O. Edfors, F. Tufvesson, and T. L. Marzetta, "Massive MIMO for next generation wireless systems," *IEEE Commun. Mag.*, vol. 52, no. 2, pp. 186–195, Feb. 2014.
- [2] L. Lu, G. Y. Li, A. L. Swindlehurst, A. Ashikhmin, and R. Zhang, "An overview of massive MIMO: Benefits and challenges," *IEEE J. Sel. Topics Signal Process.*, vol. 8, no. 5, pp. 742–758, Oct. 2014.
- [3] F. Rusek, D. Persson, B. K. Lau, E. G. Larsson, T. L. Marzetta, O. Edfors, and F. Tufvesson, "Scaling up MIMO: Opportunities and challenges with very large arrays," *IEEE Signal Process. Mag.*, vol. 30, no. 1, pp. 40–60, Jan. 2013.
- [4] G. S. Smith, "A direct derivation of a single-antenna reciprocity relation for the time domain," *IEEE Trans. Antennas Propag.*, vol. 52, no. 6, pp. 1568–1577, Jun. 2004.
- [5] B. C. Ng and C. M. S. See, "Sensor-array calibration using a maximum-likelihood approach," *IEEE Trans. Antennas Propag.*, vol. 44, no. 6, pp. 827–835, Jun. 1996.
- [6] H. Liu, L. Zhao, Y. Li, X. Jing, and T. K. Truong, "A sparse-based approach for DOA estimation and array calibration in uniform linear array," *IEEE Sensors J.*, vol. 16, no. 15, pp. 6018–6027, Aug. 2016.
- [7] X. Luo, "Multiuser massive MIMO performance with calibration errors," *IEEE Trans. Wireless Commun.*, vol. 15, no. 7, pp. 4521–4534, Jul. 2016.
- [8] W. Zhang, H. Ren, C. Pan, M. Chen, R. C. Lamare, B. Du, and J. Dai, "Large-scale antenna systems with UL/DL hardware mismatch: achievable rates analysis and calibration," *IEEE Trans. Commun.*, vol. 63, no. 4, pp. 1216–1229, Apr. 2015.
- [9] H. Wei, D. Wang, H. Zhu, J. Wang, S. Sun, and X. You, "Mutual coupling calibration for multiuser massive MIMO systems," *IEEE Trans. Wireless Commun.*, vol. 15, no. 1, pp. 606–619, Jan. 2016.
- [10] M. Petermann, M. Stefer, F. Ludwig, D. Wübben, M. Schneider, S. Paul, and K. Kammeyer, "Multi-user pre-processing in multi-antenna OFDM TDD systems with non-reciprocal transceivers," *IEEE Trans. Commun.*, vol. 61, no. 9, pp. 3781–3793, Sep. 2013.
- [11] C. Shepard, H. Yu, N. Anand, L. E. Li, T. Marzetta, R. Yang, and L. Zhong, "Argos: Practical many-antenna base stations," in *Proc. ACM Int. Conf. Mobile Comput. Netw. (Mobicom)*, Istanbul, Turkey, Aug. 2012, pp. 1–12.
- [12] A. Benzin and G. Caire, "Internal self-calibration methods for large scale array transceiver software-defined radios," in *Proc. IEEE Int. ITG Workshop Smart Antennas*, Berlin, Germany, Mar. 2017, pp. 1–8.
- [13] K. Nishimori, K. Cho, Y. Takatori, and T. Hori, "Automatic calibration method using transmitting signals of an adaptive array for TDD systems," *IEEE Trans. Veh. Technol.*, vol. 50, no. 6, pp. 1636–1640, Nov. 2001.
- [14] J. Liu, G. Vandersteen, J. Craninckx, M. Libois, M. Wouters, F. Petré, and A. Barel, "A novel and low-cost analog frond-end mismatch calibration scheme for MIMO-OFDM WLANs," in *Proc. IEEE Radio and Wireless Symp.*, San Diego, CA, Oct. 2006, pp. 219–222.
- [15] J. Vieira, F. Rusek, O. Edfors, S. Malkowsky, L. Liu, and F. Tufvesson, "Reciprocity calibration for massive MIMO: Proposal, Modeling, and Validation," *IEEE Trans. Wireless Commun.*, vol. 16, no. 5, pp. 3042–3056, May 2017.
- [16] F. Kaltenberger, H. Jiang, M. Guillaud, and R. Knopp, "Relative channel reciprocity calibration in MIMO/TDD systems," in *Proc. IEEE Future Netw. Mobile Summit*, Florence, Italy, Jun. 2010, pp. 1–10.
- [17] J. Shi, Q. Luo, and M. You, "An efficient method for enhancing TDD over the air reciprocity calibration," in *Proc. IEEE Wireless Commun. Networking Conf.*, Cancun, Quintana Roo, Mar. 2011, pp. 339–344.
- [18] R. Rogalin, O. Y. Bursalioglu, H. Papadopoulos, G. Caire, A. F. Molisch, A. Michaloliakos, V. Balan, and K. Psounis, "Scalable synchronizaiton and reciprocity calibration for distributed multiuser MIMO," *IEEE Trans. Wireless Commun.*, vol. 13, no. 4, Apr. 2014.

- [19] X. Luo, "Robust large scale calibration for massive MIMO," in *Proc. IEEE Global Commun. Conf. (GLOBECOM)*, San Diego, CA, Dec. 2015, pp. 1–6.
- [20] K. Nishimori, T. Hiraguri, T. Ogawa, and H. Yamada, "Effectiveness of implicit beamforming using calibration technique in massive MIMO system," in *Proc. IEEE Int. Workshop Electromagn. (iWEM)*, Sapporo, Japan, Aug. 2014, pp. 117–118.
- [21] H. Bolcskei, D. Gesbert, and A. J. Paulraj, "On the capacity of OFDM based spatial multiplexing systems," *IEEE Trans. Commun.*, vol. 50, no. 2, pp. 225–234, Feb. 2002.
- [22] S. M. Kay, *Fundamentals of Statistical Signal Processing: Estimation Theory*. Upper Saddle River, New Jersey, USA: Prentice Hall, 1993.
- [23] D. B. West, *Introduction to Graph Theory*, 2nd ed. Upper Saddle River, NJ, USA: Prentice Hall, 2001.